ORIGINAL RESEARCH

Numerical Experiments on Neon Soft X-Ray Optimization of AECS-PF2 Plasma Focus Device

Sh. Al-Hawat · M. Akel · S. Lee

Abstract Numerical experiments have been investigated on modified AECS-PF2 with neon filling gas using the latest version of Lee model. The model was applied to characterize the 2.8 kJ plasma focus AECS-PF2, finding a neon soft X-ray yield (Y_{sxr}) of 0.04 J in its typical operation. By numerical experiments the optimum combination of pressure of 0.57 Torr, anode length of 9 cm and anode radius of 1.57 cm was found. The optimum Y_{sxr} found also to be 0.87 J. Thus we expect to increase the neon Y_{sxr} of AECS-PF2 22-fold from its present typical operation; without changing the capacitor bank, merely by changing the electrode configuration. The Lee model code was also used to run numerical experiments on AECS-PF2 with neon gas for optimizing soft X-ray yield with reducing L_0, varying z_0 and 'a'. From these numerical experiments we expect to increase the neon Y_{sxr} of AECS-PF2 with reducing L_0, from the present 0.04 J at $L_0 = 280$ nH to maximum value of near 21 J at an achievable $L_0 = 15$ nH at the pressure 2.8 Torr.

Sh. Al-Hawat (✉) · M. Akel
Department of Physics, Atomic Energy Commission,
Damascus, P. O. Box 6091, Syria
e-mail: pscientific1@aec.org.sy

S. Lee
Institute for Plasma Focus Studies, 32 Oakpark Drive,
Chadstone, VIC 3148, Australia

S. Lee
National Institute of Education, Nanyang Technological
University, Singapore 637616, Singapore

S. Lee
INTI International University, 71800 Nilai, Malaysia

Introduction

The Plasma Focus is an efficient device for compressing and heating plasmas in a pulsed mode. In a simple, cost effective manner, by using only a conventional capacitor, the plasma focus produces plasma with high density and high temperature. Responding to the needs of modern technological advances, the plasma focus has been used as potential X-ray source for various medico-biological and industrial applications such as lithography (using ∼ 0.9–1.5 keV photons) [1–4], radiography [5, 6], microscopy (using ∼ 0.25–2.5 keV radiations) [7, 8], and micromachining (using ∼ 4 keV photons) [9]. The X-ray emission from DPF (Dense Plasma Focus) is characterized by high intensity and a wide spectral range, the emission times ranging a few to a few tens of nanoseconds for a small focus. The predominant spectral range that is actually radiated can be controlled by using a specific gas at a specific temperature. Good soft X-ray yield can be achieved by neon as a filling gas with characteristic spectral energies around 1 keV. In the last few years various efforts have been made for enhancing the X-ray yield by changing various experimental parameters such as bank energy [10], discharge current, electrode configuration (shape and material) [11, 12], insulator material and dimensions [11], gas composition and filling gas pressure [5]. Thus, soft X-ray yield optimization studies on the plasma focus devices operating over the wide range of bank energies have been one of the actively pursued fields

of plasma focus research owing to their vast possible applications.

Based on corona model, it is shown that for operation in neon, a focus pinch compression temperature of 200–500 eV (2.3×10^6–5×10^6 K) is suitable for generating H-like and He-like ions in neon plasma (therefore neon soft X-ray emissions) [13, 14]. For the UNU/ICTP PFF, Liu [13] has shown that the required end axial speed is around 6–7 cm/μs; giving an average axial speed of around 4 cm/μs. For the soft X-rays from neon operated 3.3 kJ UNU-ICTP plasma focus device it was found that 64% of soft X-ray emission can be attributed to line radiations at 922 eV (He-like alpha line) and 1,022 eV (H-like alpha line) and the remaining 36% by the rest, mainly recombination radiation, for optimized operations [15].

The Lee model code has been successfully used to perform numerical experiments to compute neon soft X-ray yield for the NX2 as a function of pressure with reasonable degree of agreement in the Y_{sxr} versus pressure curve trends, the absolute maximum yield and the optimum pressure value. The only input required is a measured total current waveform. This reasonably good agreement, against the background of an extremely complicated situation to model, moreover the difficulties in measuring Y_{sxr}, gives confidence that the model is sufficiently realistic in describing the plasma focus dynamics and soft X-ray emission for NX2 operating in Neon [10].

Numerical experiments for the UNU/ICTP PFF capacitor system using the Lee model code have shown that even more drastic shortening of anode length z_0 is required, from the original 16–7 cm; at the same time increasing the anode radius 'a' from 0.95 to 1.2 cm, to obtain an optimum yield of $Y_{sxr} = 9.5$ J. This represents a 2- to 3-fold increase in Y_{sxr} from that computed for the standard UNU/ICTP PFF [16].

In the code [17, 18] we take the neon soft X-ray yield (from H-like and He-like Neon ions) to be equivalent to line radiation yield i.e. $Y_{sxr} = Q_L$ at the following temperature range 200–500 eV. The detailed description, theory, latest code and a broad range of results of this 'Universal Plasma Focus Laboratory Facility' are available for download from ref. [18, 19].

In our previous work [17] the Lee model has been used to characterize the high inductance PF-SY1 (AECS-PF1) Plasma Focus at neon filling gas and some numerical experiments have been investigated for optimizing neon soft X-ray yield, where the maximum soft X-ray yield was found to be 0.026 J.

In this paper, for the first time, we use the latest version Lee Model RADPF5.15 K for characterization and optimization of the modified relatively low inductance AECS-PF2.

Characterization of AECS-PF2 with Neon Filling Gas

The numerical experiments were conducted on the new relatively low inductance (compared to its predecessor PF-1) low energy plasma focus device AECS-PF2 for neon soft X-ray optimization. The bank parameters were $L_0 = 200$ nH, $C_0 = 25$ μF and $r_0 = 14$ mΩ. The tube parameters were the outer radius $b = 3.2$ cm, the inner radius $a = 0.95$ cm, and the anode length $z_0 = 16$ cm. The operating parameters were $V_0 = 15$ kV, and $p_0 = 0.57$ Torr, filling neon gas.

Several experiments have been investigated on the AECS-PF2 with neon filling gas at wide range of pressures by step of 0.1 mbar to get different experimental current traces with good focus effect. By these experiments, good focusing action has been obtained in the pressure range from 0.25 to 1.25 Torr. No focus effect occurs experimentally at higher pressure. To start the numerical experiments we select a discharge current trace of the AECS-PF2 taken with a Rogowski coil at 0.57 Torr. The measured analogue current waveform at the above conditions is shown in Fig. 1.

We first digitize the measured current waveform using an open access source digitizing program [20] and then we fit the computed current waveform to the measured waveform as follows:We configure the Lee model code (version RADPF5.15 K) to operate as AECS-PF2 plasma focus using the following bank and tube parameters:Bank parameters: $L_0 = 280$ nH, $C_0 = 25$ μF, $r_0 = 25$ mΩ; tube parameters: $b = 3.2$ cm, $a = 0.95$ cm, $z_0 = 16$ cm; operating parameters: $V_0 = 15$ kV, $p_0 = 0.57$ Torr, neon gas. The following model parameters are fitted:$f_m = 0.1$,
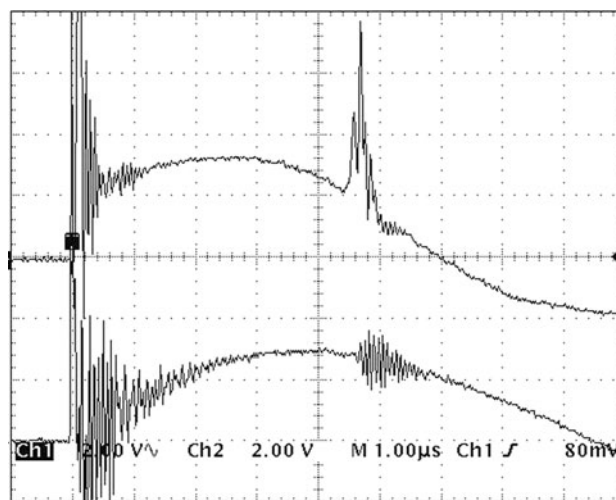

Fig. 1 The temporal evolution of voltage (*up*) and current (*down*) of the neon discharge during the plasma focus formation in AECS-PF2, (1vert. div = 2 kV for voltage; and 76.76 kA for current). $p_0 = 0.57$ Torr, $C_0 = 25$ μF, $L_0 = 200$ nH, $r_0 = 14$ mΩ, $V_0 = 15$ kV
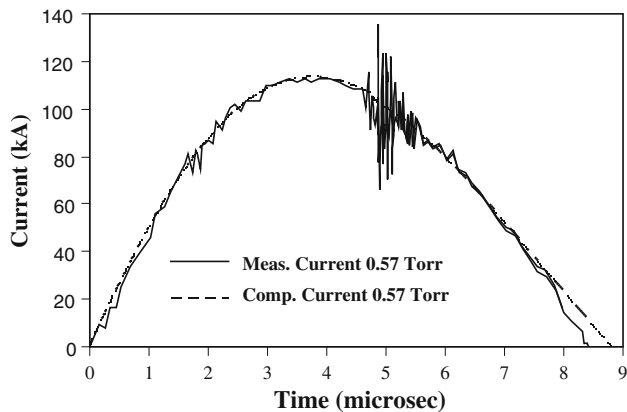
Fig. 2 Comparison of the computed current trace (*dotted line*) with the experimental one (*solid smooth line*) of the AECS-PF2 at 15 kV, 0.57 Torr at neon filling gas

Fig. 4 Computed plasma focus speeds and line radiation of the AECS-PF2 at 15 kV, 0.57 Torr at neon filling gas during radial phase

Optimizing of AECS-PF2 for Neon Soft X-Ray Emission

Soft X-Ray Yield Versus Pressure

These fitted values of the model parameters are then used for the computation of all the discharges at various pressures. The pressure was varied from 0.1 to 2.1 Torr [21]. From the Table 1, it is seen that the Y_{sxr} increases with increasing pressure until it reaches the maximum value about 0.42 J at $p_0 = 1.12$ Torr, the corresponding efficiency is about 0.015%, the end axial speed is $V_a = 4.2$ cm/µs, and the speed factor (SF) is 113.4 kA/(cm Torr$^{1/2}$). As expected as p_0 is increased, the end axial speed, the inward shock speed and the radial piston speed all reduced (Table 1). The decrease in speeds lead to lowering of plasma temperatures below that needed for soft X-ray production. Figure 5 presents the X-ray yield and temperature as functions of the pressure. It is also evident from the Table 1 that the peak value of total discharge current I_{peak} slightly decreases with decreasing pressure. This is due to increasing dynamic resistance (rate of change of plasma inductance, dL/dt gives rise to a dynamic resistance equal to 0.5 dL/dt) due to the increasing current sheath speed as pressure is decreased. We note that, on the contrary, the current I_{pinch} that flows through the pinched plasma column increases with decreasing pressure until it reaches a maximum. This is due to the shifting of the pinch time closer and closer towards the time of peak current as the current sheet moves faster and faster [16, 17]. As the pressure is decreased, the increase in I_{pinch} may be expected to favour Y_{sxr}; however there is a competing effect that decreasing pressure reduces the number density. The interaction of these competing effects will decide on the actual yield versus pressure behavior as shown in the computed results. For comparison the numerical experiments at extended range of different pressures
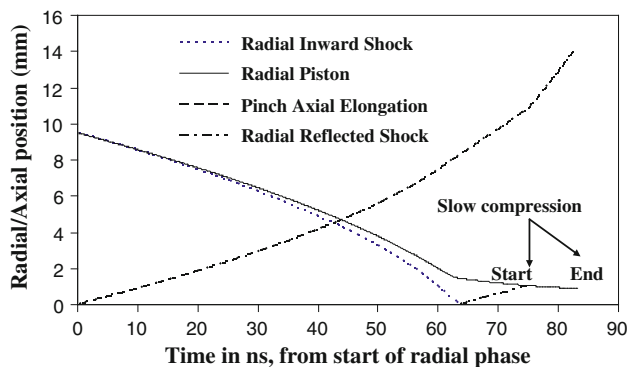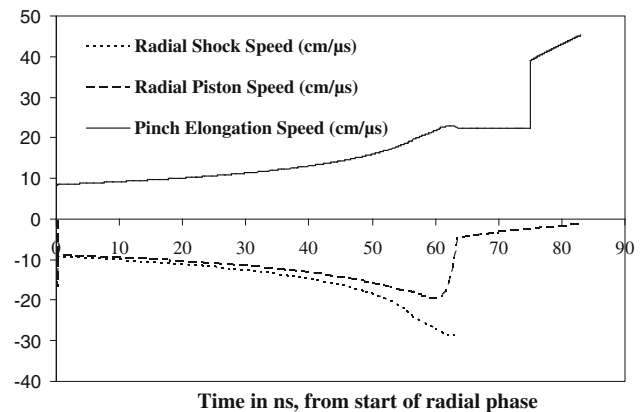

Fig. 3 Obtained plasma focus dimensions of the AECS-PF2 at 15 kV, 0.57 Torr at neon filling gas during radial phase

$f_c = 0.7$, $f_{mr} = 0.2$ and $f_{cr} = 0.7$. With these parameters, the computed total current trace agrees reasonably well with the experimental trace (Fig. 2).

This fit gives the following results: end axial speed $V_a = 5.9$ cm/µs, the speed factor (SF = $(I_0/ap_0^{1/2})$ is 156.4 kA/(cm per Torr$^{1/2}$). From Figs. 3, 4, it is seen that the plasma parameters (dimensions, speeds and line radiation) are changing slowly in the first half part of the radial inward shock phase. The final plasma column is 0.09 cm in radius, and 1.4 cm in length. The inward shock speed is steadily increasing in the inward shock phase to a final on-axis speed of $V_s = 28.7$ cm/µs and the radial piston speed is also increasing to a maximum value of $V_p = 19.6$ cm/µs and the pinch duration is about 8 ns. Also the Y_{sxr} emitted from the neon plasma is calculated at the above conditions, to be 0.039 J (see Table 1), and the corresponding wall plug efficiency is 0.0014%. The peak values of total discharge current I_{peak} is 112 kA, the pinch current I_{pinch} is 76 kA, and the focusing occurs at about 4.8 µs.

Table 1 Variation AECS-PF2 parameters with pressure at: $L_0 = 280$ nH, $C_0 = 25$ μF, $r_0 = 25$ mΩ, $V_0 = 15$ kV, RESF = 0.236, c = b/a = 3.368, $f_m = 0.1$, $f_c = 0.7$, $f_{mr} = 0.2$, $f_{cr} = 0.7$, neon gas

p_0 (Torr)	I_{peak} (kA)	I_{pinch} (kA)	V_a (cm/μs)	V_s (cm/μs)	V_p (cm/μs)	SF	Pinch duration	Y_{sxr} (J)	Efficiency %
2.1	The code unable to run								
1.90	115.2	44.4	3.02	12.2	9.8	88.0	14.8	0.000	0
1.80	115.1	47.6	3.14	13.1	10.5	90.3	13.7	0.000	0
1.70	115.0	50.6	3.27	14.1	11.3	92.8	12.5	0.000	0
1.60	114.8	53.6	3.41	15.5	12.0	95.6	11.5	0.000	0
1.50	114.7	56.5	3.55	16.8	12.8	98.6	10.8	0.000	0
1.40	114.6	59.2	3.71	18.3	13.6	101.9	10.0	0.000	0
1.30	114.4	61.9	3.88	19.9	14.2	105.6	9.2	0.000	0
1.20	114.2	64.4	4.06	21.5	14.7	109.7	8.6	0.000	0
1.15	114.1	65.6	4.16	22.5	15.0	112.0	8.2	0.000	0
1.12	114.0	66.3	4.22	23.2	15.2	113.4	8.0	0.418	0.015
1.10	114.0	66.8	4.27	23.7	15.3	114.4	7.7	0.355	0.013
1.00	113.8	69.0	4.49	24.9	15.8	119.8	7.9	0.247	0.009
0.80	113.2	72.8	5.03	25.8	16.9	133.2	8.2	0.114	0.004
0.70	112.8	74.4	5.36	26.8	17.8	141.9	8.2	0.075	0.0026
0.57	112.2	75.9	5.87	28.7	19.6	156.4	7.9	0.039	0.0014
0.50	111.7	76.4	6.21	30.1	20.9	166.3	7.6	0.026	0.0009
0.40	111.0	76.5	6.80	32.8	23.4	184.7	7.0	0.013	0.0005
0.30	109.5	75.7	7.59	35.9	26.2	210.3	6.5	0.005	0.0002
0.20	105.6	73.2	8.78	41.7	30.0	248.5	5.7	0.001	0.000036
0.10	96.2	66.8	11.04	52.7	36.8	320.1	4.6	0.000	0

(0.25–5.3 Torr) were also carried out on UNU/ICTP PF using the same fitting parameters and conditions, as reported by Saw for neon soft X-ray optimization from UNU/ICTP PF (3 kJ) device in ref. [16] and it is seen that the Y_{sxr} increases with increasing pressure until it reaches the maximum value about 3.2 J at $p_0 = 3.1$ Torr, the end axial speed being $V_a = 5.6$ cm/μs, and the speed factor (SF) is 108 kA/(cm Torr$^{1/2}$), the corresponding efficiency is about 0.1%. The peak values of total discharge current I_{peak} is 180 kA and the pinch current I_{pinch} is 110 kA. S. Lee et al. [10] by numerical experiments on NX2 plasma focus device for neon soft X-ray optimization, reported that the maximum neon soft X-ray from NX2 was found to be 20.8 J at 2.9 Torr, the end axial speed being $V_a = 5.8$ cm/μs, the speed factor (SF) is 114 kA/(cm Torr$^{1/2}$), the corresponding efficiency is 1.22%. The peak values of total discharge current I_{peak} is 370 kA and the pinch current I_{pinch} is 142 kA.

Soft X-Ray Yield Versus Pressure and Electrode Geometry

We next wish to optimize the soft X-ray yield from AECS-PF2 plasma focus with neon gas, so more numerical experiments were also carried out with the above model parameters; but varying p_0, z_0 and 'a' keeping c = b/a constant at value c = 3.368. The pressure p_0 was varied from 0.3 to 5 Torr.
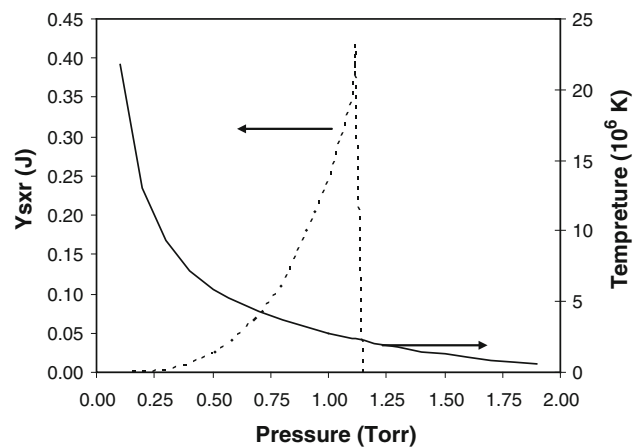

Fig. 5 The X-ray yield and temperature as functions of the pressure from AECS-PF2

The following procedure was used [17, 22, 23]:

– At each p_0, the anode length z_0 was fixed at a certain value,
– Then the anode radius 'a' was varied, till the maximum X-ray yield (Y_{sxr}) was obtained for this certain value of z_0.
– After that, we chose another value of z_0, varying the value of 'a' looking for the maximum of Y_{sxr}, until we

found the optimum combination of z_0 and 'a' for the best X-ray yield at the fixed p_0.

- Then we changed p_0 and repeated the above procedure to find the optimum combination of z_0 and 'a' corresponding to this new value of p_0. We proceeded until we had obtained the optimum combination of p_0, z_0 and 'a' for the maximum soft X-ray yield.

The numerical experiments showed that z_0 needed to be increased to optimize the Y_{sxr} (see Table 2). Thus whilst external inductance L_0 is fixed at a constant value and an axial section inductance L_a is increased due to increasing the anode length, the pinch inductance L_p is reduced due to decreasing the pinch length.

The optimized results for each value of p_0 are shown in Table 2. The table shows that as p_0 is increased, anode length z_0 rises and inner radius 'a' decreases with each increase in p_0, while the soft X-ray yield slightly increases with increasing p_0 until it reaches a maximum value of 0.874 J at $p_0 = 0.57$ Torr; then the Y_{sxr} decreases with further pressure increase.

Figure 6 shows X-ray yield as function of p_0, with the plasma focus operated at the optimum combination of z_0 and 'a' corresponding to each p_0. Figure 7 shows the corresponding optimum z_0 and 'a' as functions of pressure. As p_0 was increased; the total current (I_{peak}) and the pinch current (I_{pinch}) slightly increased until they reached their maximum values, then slightly decreased with further increase in p_0 (see Fig. 8).

From the numerical experiments for AECS-PF2 with $L_0 = 280$ nH, $C_0 = 25$ µF, $r_0 = 25$ mΩ, $V_0 = 15$ kV we have thus found the optimum combination of p_0, z_0 and 'a' for neon Y_{sxr} as 0.57 Torr, 9 and 1.567 cm respectively,
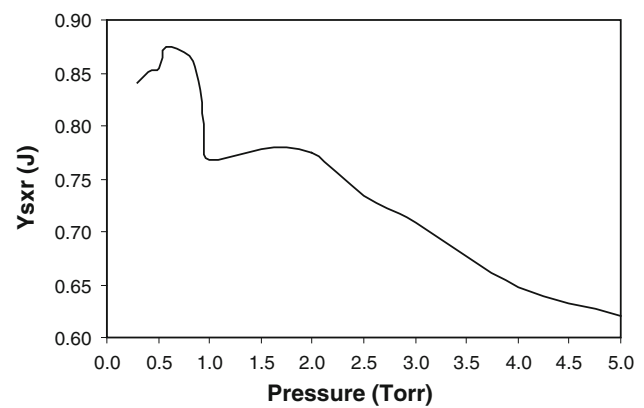

Fig. 6 The X-ray yield from AECS-PF2 as function of pressure, anode length and inner radius (Y_{sxr} vs. p_0, z_0 and 'a')
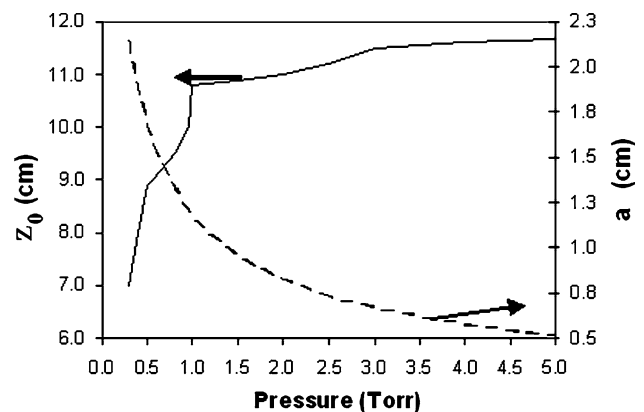

Fig. 7 Variation of the anode length and inner radius as functions of pressure

Table 2 X-ray yield optimization from AECS-PF2 for each value of p_0 varying z_0 and 'a' at filling neon gas

p_0 (Torr)	z_0 (cm)	a (cm)	I_{peak} (kA)	I_{pinch} (kA)	Y_{sxr} (J)	V_a (cm/µs)	a_{min} (cm)	z_{max} (cm)
0.30	7.0	2.15	113.9	77.4	0.841	3.4	0.17	3.0
0.40	8.0	1.87	114.7	77.8	0.851	3.5	0.14	2.6
0.50	8.9	1.67	114.8	77.4	0.854	3.6	0.13	2.3
0.57	9.0	1.567	114.8	77.5	0.874	3.6	0.12	2.2
0.80	9.5	1.320	114.8	77.3	0.865	3.6	0.10	1.9
0.90	9.8	1.240	114.8	77.1	0.843	3.7	0.09	1.7
0.95	10.0	1.200	114.7	76.9	0.802	3.7	0.09	1.7
1.00	10.8	1.154	114.7	75.7	0.767	3.7	0.09	1.6
1.50	10.9	0.946	114.7	75.9	0.778	3.7	0.07	1.3
2.00	11.0	0.820	114.7	75.9	0.775	3.7	0.06	1.2
2.50	11.2	0.730	114.7	75.8	0.735	3.7	0.06	1.0
3.00	11.5	0.665	114.7	75.3	0.708	3.8	0.05	0.9
4.00	11.6	0.574	114.6	75.3	0.647	3.8	0.04	0.8
5.00	11.7	0.515	114.7	75.2	0.621	3.8	0.04	0.7

$L_0 = 280$ nH, $C_0 = 25$ µF, $r_0 = 25$ mΩ, $V_0 = 15$ kV, RESF = 0.236, c = b/a = 3.368, $f_m = 0.1$, $f_c = 0.7$, $f_{mr} = 0.2$, $f_{cr} = 0.7$
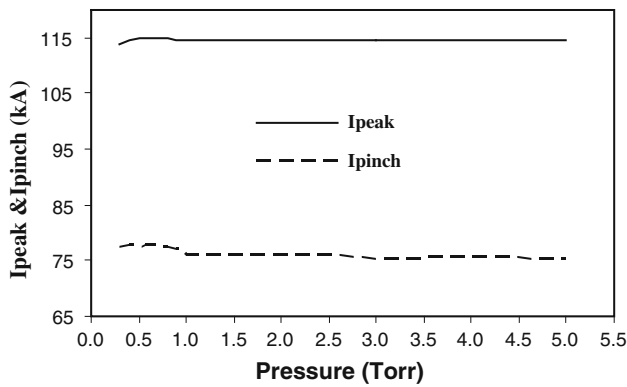
Fig. 8 Effect on currents I_{peak} and I_{pinch} as p_0 is increased from 0.3 to 5 Torr

with the outer radius b = 5.3 cm. This combination gives Y_{sxr} = 0.874 J. We also note that at this optimum configuration I_{peak} = 115 kA, I_{pinch} = 78 kA, and the end axial speed is of 3.6 cm/μs. Comparing with our earlier work on PF-SY1 [17], which has been shown that with the present capacitor bank, PF-SY1 plasma focus has a low maximum Y_{sxr} at about 0.026 J, while it can be noticed that the optimum soft X-ray yield from AECS-PF2 becomes higher (about 1 J), this is due to the lower value of L_0, and consequently higher pinch current value I_{pinch}.

Thus our results correspond with earlier numerical experiments carried out by Saw et al. [16] on UNU/ICTP PF, which have shown that shortening of anode length z_0 is required, from the original 16–7 cm; at the same time increasing the anode radius 'a' from 0.95 to 1.2 cm and consequently the outer radius "b" from 3.2 to 4 cm, to obtain an optimum yield of Y_{sxr} = 8 J.

To find the "practical optimum" we continue with the numerical experiments, keeping b = const at the original value of 3.2 cm; changing 'a' to 1.567 cm with z_0 = 9 cm; and varying pressure. The results are shown in Table 3.

This gives us a practical optimum configuration of b = 3.2 cm (unchanged from the original cathode radius of the standard AECS-PF2), a = 1.567 cm, z_0 = 9 cm, giving a practical optimum yield of 0.924 J at a p_0 of 0.58 Torr. The slightly higher yield compared with that in Table 1 is due to the decreased ratio "c" from 3.4 to 2. An earlier study has shown that reducing c, down to certain limits, has a beneficial effect in the case of neutron production operating in deuterium, and we have also confirmed through numerical experiments that this effect is also observed for neon Y_{sxr}. It would be interesting to see if the predicted 23-fold increase in Y_{sxr} going from the standard AECS-PF2 anode to the optimized anode may be achieved in the laboratory.

Here, also we can compare our results with practical optimum configuration carried out by Saw et al. [16] on UNU/ICTP PF (the anode length z_0 = 7 cm; the anode radius a = 1.2 cm, b = 3.2 cm, and Y_{sxr} = 9.5 J), which would increase the neon soft X-ray yield by 2- to 3-fold from that computed for the standard UNU/ICTP PF.

Soft X-Ray Yield Versus Inductance and Electrode Geometry

To optimize the soft X-ray yield from AECS-PF2 with neon gas, varying L_0, z_0 and "a" keeping "c" and RESF constant (RESF = stray resistance/surge impedance). The external inductance L_0 was varied from 280 to 3 nH.

Table 3 Variation AECS-PF2 parameters with pressure at: L_0 = 280 nH, C_0 = 25 μF, r_0 = 25 mΩ, V_0 = 15 kV, RESF = 0.236, c = b/a = 3.334, b = 3.2, a = 0.96, z_0 = 6.5, f_m = 0.1, f_c = 0.7, f_{mr} = 0.2, f_{cr} = 0.7, neon gas

p_0 (Torr)	I_{peak} (kA)	I_{pinch} (kA)	V_a (cm/μs)	V_s (cm/μs)	V_p (cm/μs)	Y_{sxr} (J)
0.30	106	74	5.8	25.9	16.8	0.123
0.40	110	76	5.3	25.2	16.1	0.273
0.50	113	78	4.9	24.8	15.5	0.509
0.55	114	78	4.7	23.7	15.2	0.723
0.57	114	78	4.7	23.2	15.1	0.836
0.58	114	78	4.7	22.9	15.1	0.924
0.59	114	79	4.6	22.6	15.0	0.170
0.60	114	79	4.6	22.6	15.0	0.000
0.70	115	79	4.3	20.8	14.5	0.000
0.80	116	79	4.1	19.6	14.0	0.000
0.90	116	79	3.9	18.3	13.6	0.000
1.00	116	79	3.8	17.2	13.0	0.000
1.20	117	78	3.5	15.6	12.1	0.000
1.50	117	76	3.2	13.5	10.8	0.000
1.80	117	73	2.9	12.3	9.8	0.000

The following procedures were used [17, 23, 24]:

At each L_0, the pressure was fixed at constant value (in our case $p_0 = 2.8$ Torr) and also the anode length was fixed at a certain value:

- Then the inner radius "a" was varied, whilst keeping c = 3.368, until the maximum X-ray yield was obtained for this certain value of z_0.
- After that we chose another value of z_0, varying "a" until maximum X-ray yield and so on, until we have obtained the combination of z_0 and "a" for the best maximum X-ray yield at a fixed L_0 (Y_{sxr} vs. z_0 and "a" at fixed L_0 and p_0).
- We repeated the above procedure for progressively smaller L_0 until $L_0 = 3$ nH.

The influence of L_0 reduction on the total current traces using RADPF5.15 K was investigated. For example it was found that reducing L_0 increases the total current from $I_{peak} = 115$ kA at $L_0 = 280$ nH to $I_{peak} = 410$ kA at $L_0 = 15$ nH (see Table 4). As L_0 was reduced, I_{peak} increased; "a" is necessarily increased leading to longer pinch length (Z_{max}), hence a bigger pinch inductance L_p. At the same time because of the reducing current drive time, z_0 needed to be reduced. The geometry moved from a long thin Mather-type to a shorter fatter one (see Table 4). Thus whilst L_0 and axial section inductance L_a reduced, the pinch inductance L_p increased due to increased pinch length.

At each L_0, after z_0 was varied, the inner radius "a" was adjusted to obtain the optimum X-ray yield, which corresponds closely to the largest I_{pinch}.

The soft X-ray optimization for each value of L_0, varying z_0 and "a" is shown in Table 4. The table shows that as L_0 is reduced, I_{peak} increases with each reduction in L_0 with no sign of any limitation as function of L_0. However, I_{pinch} reaches a maximum of 214 kA at $L_0 = 5$ nH,

then it decreases with each reduction in L_0. Thus I_{peak} doesn't show any limitation as L_0 is progressively reduced. However I_{pinch} has a maximum value. This pinch current limitation effect is not a simple, but it is a combination of the two complex effects: the interplay of the various inductances involved in the plasma focus processes abetted by the increasing coupling of C_0 to the inductive energetic processes, L_0 is reduced. From Fig. 9 it is clearly shown the difference between I_{pinch} and I_{peak}.

From Table 4 it can be seen, that as L_0 decreased, the soft X-ray yield increases until it reaches a maximum value of 22 J at $L_0 = 15$ nH; beyond which the soft X-ray yield does not increase with reducing L_0. Thus with decreasing L_0 the pinch current I_{pinch} and the soft X-ray yield show limitation. The obtained results confirm the pinch current limitation effect in neon plasma focus, and consequently the soft X-ray yield. Figure 10 represents I_{pinch} and X-ray limitation effects in neon plasma focus at 2.8 Torr as L_0 is reduced from 280 to 3 nH.

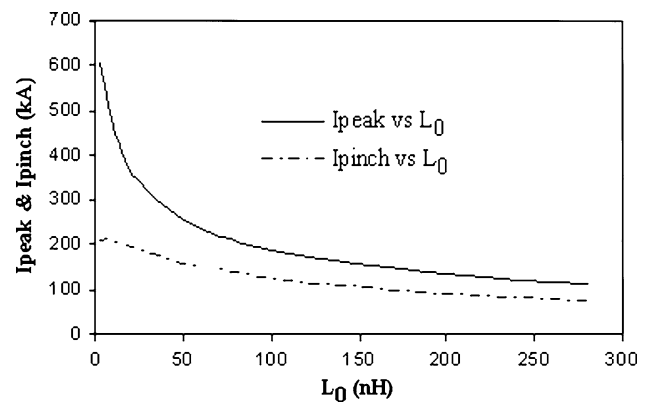Looking at Table 4, it is noticed that as L_0 was progressively reduced, "a" had to be progressively increased

Fig. 9 Effect of L_0 reduction on currents (computed) AECS-PF2 at 15 kV, 2.8 Torr of Neon

Table 4 For each L_0 the optimization combination of z_0 and 'a' were found and are listed here

L_0 (nH)	z_0 (cm)	a (cm)	b (cm)	I_{peak} (kA)	I_{pinch} (kA)	a_{min} (cm)	Z_{max} (cm)	V_a (cm/μs)	Y_{sxr} (J)
280	8.00	0.727	2.45	115	79	0.05	1.0	3.45	0.94
200	7.00	0.842	2.84	135	92	0.06	1.2	3.52	1.66
100	4.50	1.125	3.79	186	125	0.08	1.6	3.57	5.16
50	4.00	1.400	4.73	256	158	0.10	2.0	4.02	11.62
25	2.80	1.640	5.52	340	190	0.14	2.4	4.50	18.72
20	2.50	1.693	5.70	369	198	0.16	2.5	4.72	20.35
15	2.40	1.732	5.83	410	205	0.17	2.6	5.15	21.77
10	2.00	1.760	5.93	464	212	0.20	2.7	5.71	21.40
5	1.97	1.749	5.89	556	214	0.25	2.7	7.12	16.14
3	1.96	1.705	5.74	608	211	0.26	2.6	8.16	13.19

Bank parameters: $L_0 = 280$ nH, $C_0 = 25$ μF, $r_0 = 25$ mΩ; tube parameter: c = b/a = 3.368; model parameters: $f_m = 0.1$, $f_c = 0.7$, $f_{mr} = 0.2$, $f_{cr} = 0.7$; operating at 2.8 Torr neon gas, $V_0 = 15$ kV
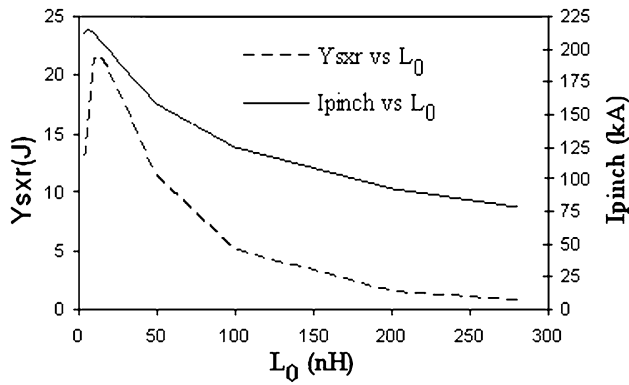
Fig. 10 The X-ray yield and I_{pinch} (computed) versus L_0 (280–3 nH) at 15 kV, 2.8 Torr of Neon
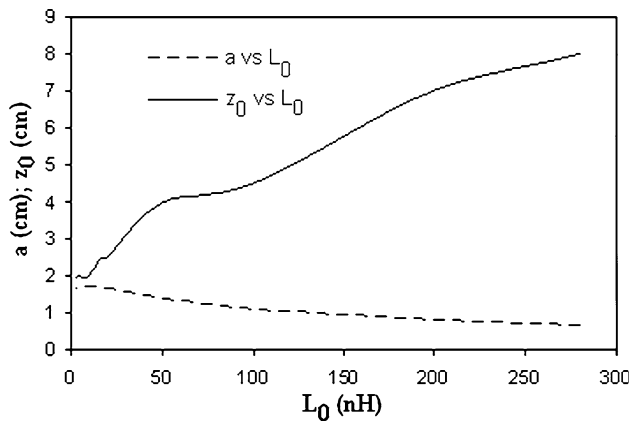

Fig. 11 Effect on the anode length and inner radius (computed) as L_0 is reduced at 15 kV, 2.8 Torr of Neon

and z_0 progressively decreased. Also the plasma pinch dimensions (pinch radius a_{min} and pinch length Z_{max}) increased as L_0 was reduced. Figure 11 show a variation of plasma focus dimensions as L_0 was reduced in AECS-PF2 of 15 kV and 2.8 Torr neon.

Based on the obtained results of these sets of numerical experiments on AECS-PF2 with neon gas, we can say that to improve the soft X-ray yield, L_0 should be reduced to a value around 15–25 nH (which is an achievable range incorporating low inductance technology, below which the pinch current I_{pinch} and the soft X-ray yield Y_{sxr} would not be improved much, if at all. These experiments confirm the pinch current limitation effect, and consequently the soft X-ray yield for the neon plasma focus. Finally, we would like to emphasize that we, practically, have no intention (or ambition) to go below 15–25 nH, but in our numerical experiments using RADPF5.15 K we go down to a low values of L_0 (10–3 nH) just to find the pinch current limitation effect.

In the Table 5, for comparison, we list the physical parameters associated with the collection of systems under consideration. The speed factor SF, the energy density parameter ($28E/a^3$) and energy per mass parameter ($E/a^3 p_0$) are listed for various PF devices, E is the stored energy in the capacitor bank, I_{peak} is the peak current, "a" the anode radius and p_0 is the gas filling pressure for the maximum X-ray yield (Y_{sxr}). From this table, it can be seen that, the energy density parameter, introduced by Soto [27, 28] as a way to compare different PF devices, has a value of the order of $(0.7–9.6) \times 10^{10}$ J m^{-3} for all the experimentally optimized machines listed. The drive parameter has practically the same value for all the experimentally optimized machines listed (78–118 kA cm^{-1} Torr$^{-1/2}$). A new parameter related to the energy per mass, introduced also by Soto [29], 'energy per mass parameter' $E/a^3 p_0$ has a value of the order of $(0.024–8.16) \times 10^9$ J m^{-3} Torr^{-1} for all the experimentally optimized machines listed. So we can say that the drive parameter is practically constant for all these listed plasma focus devices whilst the other two parameters vary by more than one order (for the energy parameter) and more than two orders for the so-called 'energy per mass' parameter. This means that for design

Table 5 The speed factor SF and the density energy parameter ($28E/a^3$) are listed for various PF devices, E is the stored energy in the capacitor bank, I_{peak} is the peak current, a the anode radius and p_0 the neon gas filling pressure for the maximum X-ray yield

Device (ref.) location	E (kJ)	a (cm)	I_{peak} (kA)	p_0 (Torr Neon)	Energy density parameter $28E/a^3$ (J m^{-3})	SF (kA Torr$^{-1/2}$ cm^{-1})	Energy per mass parameter $E/a^3 p_0$ (J m^{-3} Torr^{-1})	Y_{sxr} (J)
AECS-PF1 [17]–Syria	2.8	0.95	47	0.4	9.14×10^{10}	78.22	8.16×10^9	0.026
AECS-PF2 [*]–Syria	2.8	0.95	115	1.12	9.14×10^{10}	114.4	2.9×10^9	0.42
UNU/ICTP PFF [16]–Singapore	2.94	0.95	180	3.3	9.6×10^{10}	104.3	1.04×10^9	3.92
NX2 [10]–Singapore	1.7	1.9	370	2.9	0.694×10^{10}	114.35	0.024×10^9	20.8
PF [25]–Pakistan	2.3	0.9	184	3	8.834×10^{10}	118.3	1.05×10^9	2.3
PF [26]–Iran	2.4	1.39	170	1.83	2.5×10^{10}	90	0.488×10^9	5.45

* This work

purposes the speed factor is the useful one whilst the other two parameters are less than useful. Moreover it can be shown that the speed factor is equivalent to the energy per unit mass of the plasma. Hence the E/a^3p_0 factor is not even a true 'energy per mass' pertaining to the plasma focus.

Conclusions

The Lee model code was applied to characterize the AECS-PF2 Plasma Focus, finding a maximum neon soft X-ray yield (Y_{sxr}) of 0.42 J, merely by changing the operating pressure. The neon soft X-ray optimum combination of AECS-PF2 was found to be (pressure = 0.57 Torr, anode length = 9 cm and anode radius = 1.57 cm). The optimum Y_{sxr} was 0.87 J.

Numerical experiments have been invistegated on AECS-PF2 with neon gas for optimizing soft X-ray yield with reducing L_0, varying z_0 and 'a'. From these numerical experiments we expect to increase the neon Y_{sxr} of AECS-PF2 with reducing L_0, up to 21 J at the operating pressure 2.8 Torr.

References

1. D. Wong, A. Patran, T.L. Tan, R.S. Rawat, P. Lee, IEEE Trans. Plasma Sci. **32**, 2227 (2004)
2. R. Petr, A. Bykanov, J. Freshman, D. Reilly, J. Mangano, M. Roche, J. Dickenson, M. Burte, J. Heaton, Rev. Sci. Instrum. **75**, 2551 (2004)
3. Y. Kato, I. Ochiai, Y. Watanabe, S. Murayama, J. Vac. Sci. Technol. B **6**, 195 (1988)
4. S. Lee, P. Lee, G. Zhang, X. Feng, V.A. Gribkov, L. Mahe, A. Serban, T.K.S. Wong, IEEE Trans. Plasma Sci. **26**, 1119 (1998)
5. F.N. Beg, I. Ross, A. Lorena, J.F. Worley, A.E. Dangor, M.G. Hanies, J. Appl. Phys. **88**, 3225 (2000)
6. S. Hussain, M. Shafiq, R. Ahmad, A. Waheed, M. Zakaullah, Plasma Sources Sci. Technol. **14**, 61 (2005)
7. F. Castillo-Mejia, M.M. Milanese, R.L. Moroso, J.O. Pouzo, M.A. Santiago, IEEE Trans. Plasma Sci. **29**, 921 (2001)
8. R.S. Rawat, T. Zhang, G.J. Lim, W.H. Tan, S.J. Ng, A. Patran, S.M. Hassan, S.V. Springham, T.L. Tan, M. Zakaullah, S. Lee, P. Lee, J. Fusion Energ. **23**, 49 (2004)
9. V.A. Gribkov, A. Srivastava, P.L.C. Keat, V. Kudryashov, S. Lee, IEEE Trans. Plasma Sci. **30**, 1331 (2002)
10. S. Lee et al., Plasma Phys. Control. Fusion **51**, 105013 (2009)
11. M. Zakaullah, K. Alamgir, M. Shafiq, S.M. Hassan, M. Sharif, S. Hussain, A. Waheed, Plasma Sources Sci. Technol. **11**, 377 (2002)
12. H. Bhuyan, S.R. Mohanty, N.K. Neog, S. Bujarbarua, R.K. Rout, J. Appl. Phys. **95**, 2975 (2004)
13. M.H. Liu, Soft X-ray from compact plasma focus. PhD Thesis, School of Science, Nanyang Technological University, December (1996)
14. S. Bing, Plasma dynamics and X-ray emission of the plasma focus. PhD Thesis NIE ICTP Open Access Archive: http://eprints.ictp.it/99/, (2000)
15. M.H. Liu et al., IEEE Trans. Plasma Sci. **26**, 135–140 (1998)
16. S.H. Saw, et al., IEEE Trans. Plasma Sci. **37**(7), 1276–1282 (2009)
17. M. Akel, Sh. Al-Hawat, S. Lee, J. Fusion Energ. **30**(1), 39–47 (2011)
18. S. Lee, Radiative dense plasma focus computation package: RADPF", http://www.intimal.edu.my/school/fas/UFLF/. http://www.plasmafocus.net/IPFS/modelpackage/File1RADPF.htm, (2011)
19. Sh. Al-Hawat, S. Saloum, Contrib. Plasma Phys. **49**(1–2), 5–14 (2009)
20. http://sourceforge.net/project/showfiles.php?groupid=67696&packageid=130007&releaseid=500277, (2010)
21. Sh. Al-Hawat, M. Akel, S. Lee, S.H. Saw, Model parameters versus gas pressure in two different plasma focus devices operated in argon and neon. J. Fusion Energ. (2011). doi:10.1007/s10894-011-9414-3
22. M. Akel, Sh. Al-Hawat, S. Lee, J. Fusion Energ. **28**(4), 355–363 (2009)
23. M. Akel, Sh. Al-Hawat, S.H. Saw, S. Lee, J. Fusion Energ. **29**, 223–231 (2010)
24. M. Akel, S. Al-Hawat, S. Lee, J. Fusion Energ. **29**, 1 (2010)
25. M. Zakaullah, et al., J. Fusion Energ. **19**(2), June 2000 (q 2002)
26. M. Habibi, R. Amrollahi, M. Attaran, J. Fusion Energ. **28**(1), 130–134 (2009)
27. L. Soto, Plasma Phys. Control. Fusion **47**, A361 (2005)
28. P. Silva, L. Soto, W. Kies, J. Moreno, Plasma Sources Sci. Technol. **13**, 329 (2004)
29. L. Soto, C. Pavez, A. Tarife, J. Moreno, F. Veloso, Plasma Sources Sci. Technol. **19**, 055017 (2010)